High-throughput powder diffraction measurement system consisting of multiple MYTHEN detectors at beamline BL02B2 of SPring-8

S. Kawaguchi, M. Takemoto, K. Osaka, E. Nishibori, C. Moriyoshi, Y. Kubota, Y. Kuroiwa, and K. Sugimoto

Citation: Review of Scientific Instruments **88**, 085111 (2017); doi: 10.1063/1.4999454
View online: http://dx.doi.org/10.1063/1.4999454
View Table of Contents: http://aip.scitation.org/toc/rsi/88/8
Published by the American Institute of Physics

High-throughput powder diffraction measurement system consisting of multiple MYTHEN detectors at beamline BL02B2 of SPring-8

S. Kawaguchi,[1] M. Takemoto,[1] K. Osaka,[2] E. Nishibori,[3] C. Moriyoshi,[4] Y. Kubota,[5] Y. Kuroiwa,[4] and K. Sugimoto[1,a)]

[1]*Research and Utilization Division, Japan Synchrotron Radiation Research Institute (JASRI), SPring-8, 1-1-1 Kouto, Sayo-cho, Sayo-gun, Hyogo 679-5198, Japan*
[2]*Industrial Application Division, Japan Synchrotron Radiation Research Institute (JASRI), SPring-8, 1-1-1 Kouto, Sayo-cho, Sayo-gun, Hyogo 679-5198, Japan*
[3]*Faculty of Pure and Applied Sciences, TIMS and CiRfSE, University of Tsukuba, Tsukuba, Ibaraki 305-8571, Japan*
[4]*Graduate School of Science, Hiroshima University, Higashihiroshima, Hiroshima 739-8526, Japan*
[5]*Department of Physical Science, Osaka Prefecture University, Sakai, Osaka 599-8531, Japan*

(Received 1 May 2017; accepted 7 August 2017; published online 23 August 2017)

In this study, we developed a user-friendly automatic powder diffraction measurement system for Debye–Scherrer geometry using a capillary sample at beamline BL02B2 of SPring-8. The measurement system consists of six one-dimensional solid-state (MYTHEN) detectors, a compact auto-sampler, wide-range temperature control systems, and a gas handling system. This system enables to do the automatic measurement of temperature dependence of the diffraction patterns for multiple samples. We introduced two measurement modes in the MYTHEN system and developed new attachments for the sample environment such as a gas handling system. The measurement modes and the attachments can offer *in situ* and/or time-resolved measurements in an extended temperature range between 25 K and 1473 K and various gas atmospheres and pressures. The results of the commissioning and performance measurements using reference materials (NIST CeO_2 674b and Si 640c), V_2O_3 and Ti_2O_3, and a nanoporous coordination polymer are presented. *Published by AIP Publishing.* [http://dx.doi.org/10.1063/1.4999454]

I. INTRODUCTION

X-ray powder diffraction has been widely used in phase identification and structure characterization of solid-state materials in atomic level. Synchrotron radiation X-ray powder diffraction (SR-XRPD) can be useful at reducing the measurement time and obtaining high angular and spatial resolution data. Hence, so far many types of powder diffractometers have been developed around the world.[1–7] At beamline BL02B2 of third-generation synchrotron radiation facility SPring-8, the large Debye–Scherrer camera with a two-dimensional (2D) imaging plate (IP) detector was developed for accurate powder diffraction data collection.[2] This instrument has been contributing in studies of the maximum-entropy-method charge densities of a wide range of materials.[8–11] Recently, the diffractometer having the space between the sample and IP detector all in vacuum has been developed at the third-generation high-brilliant storage ring PETRA III, and high-resolution data with very low-background level can be successfully collected.[7] However, there is a disadvantage that the temporal resolution of IP detectors is largely limited by the readout time, which is typically a few minutes. This limitation makes it difficult to satisfy an increasing demand for characterization techniques including time-resolved measurements that can be applied to many kinds of samples and/or in various sample environments as easily and rapidly as possible.

Recently, one-dimensional (1D) Si micro-strip MYTHEN detectors, which were developed at the Swiss Light Source,[12–14] have been used at many synchrotron facilities, e.g., the Swiss Light Source (24 modules; it covers 120° of the scattering angle 2θ),[15,16] Australian Synchrotron (16 modules; 80° in 2θ),[17] and Diamond (18 modules; 90° in 2θ).[18] The MYTHEN detectors possess characteristics such as high efficiencies, large dynamic ranges, small sizes of their Si micro-strips, and very short diffracted intensity readout times. Therefore, the MYTHEN detectors are well suited for high-throughput, time-resolved measurements.

To construct such an advanced high-throughput and user-friendly measurement system, we developed a new diffractometer consisting of multiple MYTHEN detectors, a compact auto-sampler, wide-range temperature control systems, and a gas handling system at beamline BL02B2 of SPring-8. This measurement system has single-step and double-step measurement modes, and the system can perform the SR-XRPD measurement fully automatically. The measurement can be carried out at temperatures ranging from 90 K to 1173 K. In addition, these developed instruments are available for the IP detector. It can be easily and quickly switched between multiple MYTHEN and IP detectors without changing the experimental conditions. Finally, we successfully developed a user-friendly SR-XRPD measurement system for versatile measurement techniques, e.g., high-throughput, time-resolved, and accurate diffraction. This paper presents the design and experimental verification of the new MYTHEN detector system, which has been incorporated with the existing apparatus.

a)Electronic mail: ksugimoto@spring8.or.jp

II. DETECTOR SYSTEM

All of the experiments and measurements were conducted at the bending-magnet source beamline BL02B2 of the third-generation synchrotron facility SPring-8 in Japan. The first optical component of this beamline is a total-reflection Si mirror coated by both Pt and Ni, which is used to collimate the X-rays and eliminate the higher harmonics.[19] A double Si (111) monochromator follows the mirror. In this configuration, X-rays with energies of 12–37 keV are available, and the energy resolution $\Delta E/E$ is approximately 2×10^{-4}. The beam dimensions at the sample position are generally 0.5 mm (vertical, V) × 3.0 mm (horizontal, H). The experimental station is equipped with a large Debye-Scherrer camera. The camera consists of a two-circle diffractometer and IP and serves as an X-ray detector.[2] The investigated multi-module diffractometer in this study, which is depicted in Figs. 1(a) and 1(b), consists of six MYTHEN 1K detectors (Dectris Ltd., Baden, Switzerland). We installed it in the experimental hutch of beamline BL02B2 without the removal of the IP cassette in order to easily switch between IP and six MYTHEN 1K detectors. The latter are 1D X-ray detectors operating in single-photon-counting mode, and each module is flat and consists of 1280 Si micro-strips with a 50-μm-pitch that serve as X-ray sensors. To enable high energy X-ray photons to be counted with better efficiency, one 1-mm-thick Si sensor was installed. We have mechanically and carefully adjusted the distance of the diffractometer center-to-module center and the module rotation for each module using laser displacement sensors. The details of MYTHEN detectors are described in the literature.[12–16] A receiving slit [8.0 mm (V) × 2.5 mm (H)] is mounted on the front of each detector and shapes the X-ray profile appropriately by relaxing the axial divergence effect. A photograph and schematic illustration of the assembled diffractometer and multiple MYTHEN detectors are provided in Figs. 1(c) and 1(d), respectively. The detectors are located in an Al cover, which has an Al-coated Mylar X-ray window. In the experiments described in this report, the distance between the sample and detector was 477.46 mm, and the angular interval between the centers of the adjacent detector modules was 12.5°. The 2θ coverage of each detector module was 7.63°, and the angular resolution was approximately 0.006° per channel. The gaps between the modules were 4.87°. For this detector arrangement, 2θ ranged from 2° to 78°. In order to obtain a continuous powder diffraction, the data obtained at two 2θ positions are typically combined to fill the gaps between the detector modules. In this report, we call this scanning mode "double-step mode." After the diffraction measurements were performed at the first 2θ position, the 2θ axis was rotated by 6.25°, and diffraction measurements were acquired at the second angle. Hence, the overlap regions, $(7.63 - 4.87)°/2 = 1.38°$ from the edge of each module, were generated by the double measurements. The large overlap regions are used to combine the data at the two positions into continuous diffraction data and reduce the various errors. Figure 2(a) illustrates the relationship of the angular intervals of the MYTHEN detectors. Thus, the whole powder diffraction data are obtained by combining the data collected at both the first and second 2θ positions.

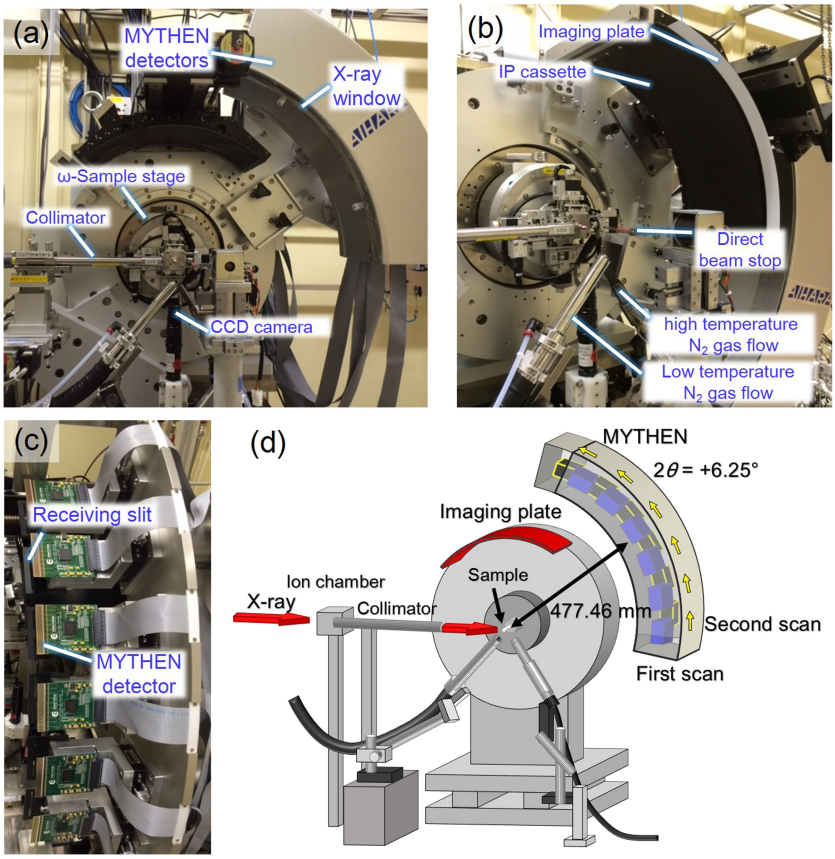

FIG. 1. (a) Photograph of the powder diffractometer equipped with six MYTHEN detectors. (b) Photograph of the IP measurement mode. (c) Assembly of six MYTHEN modules inside the detector cover. (d) Schematic illustration of the assembled diffractometer and multiple MYTHEN detectors.

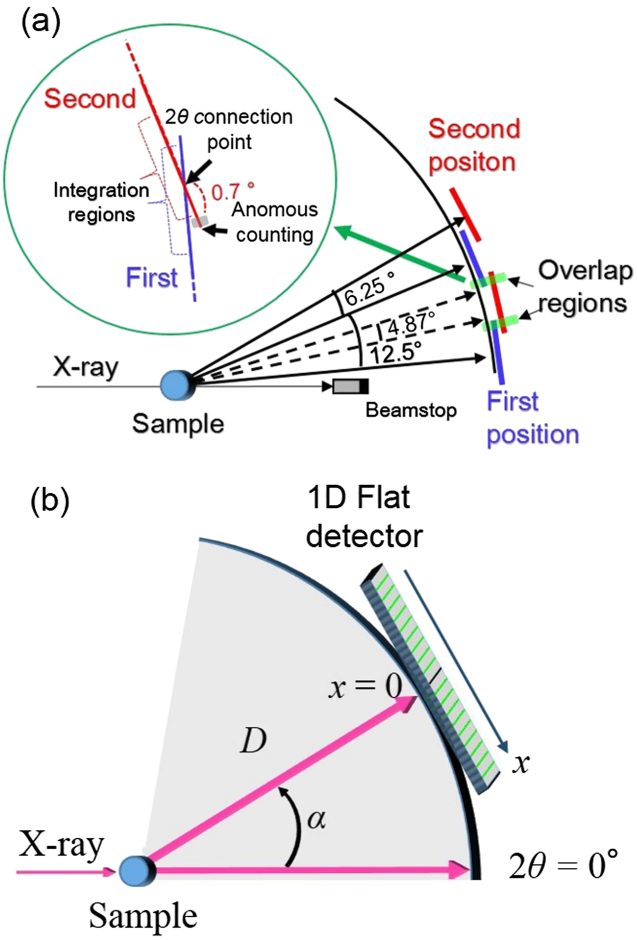

FIG. 2. Relationships between (a) detector modules and angular intervals and (b) between a channel and position in the 1D detector.

This double-step mode can be used to measure complete X-ray powder diffraction patterns with wide d-spacings.

For a flat 1D detector, the detector center and accurate coordinates for each channel are determined from the specific detector design, calibration, and spatial correction. The channel position of the flat 1D detector in diffraction space can be defined as shown in Fig. 2(b) and Eq. (1). The detector is located at a distance D from the sample with the swing angle α. The center of the detector is the intersection of the detector plane with $2\theta = 0°$ when $\alpha = 0°$. The position of a channel in the detector is defined by its coordinate, where the detector center is defined as $x = 0$. The diffraction angle 2θ for a channel at x can be given by

$$2\theta = \cos^{-1}\frac{x\sin\alpha + D\cos\alpha}{\sqrt{D^2 + x^2}} \qquad (0 < 2\theta < \pi)\,. \qquad (1)$$

In this diffractometer system, 2θ errors can occur due to the fact that detector surfaces were flat and mechanical misarrangement of the detectors.[20,21] The effects of the flat detector surfaces can be calculated geometrically without approximation; however mechanical misarrangement, namely, deviations of the detector centers and tilting of the detectors from their designed positions, can cause significant 2θ errors. Hence, 2θ correction was performed for each MYTHEN module by considering the camera length L, rotation angle R, offset angle $\Delta 2\theta$, and offset shift S, whose meaning is illustrated in Fig. 3. The appropriate parameters for each detector were obtained by fitting Gaussian profiles to the diffraction data of the standard reference materials (SRMs) CeO_2 674b and Si 640c (National Institute of Standards and Technology). All misalignment parameters, L, R, $\Delta 2\theta$, and S, were independently refined using the least-squares technique at 12 positions in 2θ (2×6 modules) for the double-step mode. All refinements were converged 5–10 times, and the correction parameters were obtained. As shown in Fig. 4(a), the differences from the ideal positions are negligible, but the whole pattern fitting results are significantly affected before data corrections. The camera length of our diffractometer was 477.4 mm. Therefore, the small mechanical deviation greatly contributes to the 2θ errors, especially near the edge of the module. Moreover, the threshold setting of the MYTHEN modules is necessary to calibrate the diffraction intensities. Details of the correction are introduced in the literature.[15,18] The intensities for all modules were tested by the measurements of the CeO_2 sample using various X-ray energies. Figures 4(b) and 4(c) show the intensities and full-width at half-maximum (FWHM) for the (111) and (200) reflections of CeO_2 observed at the center and edge channels of a module. The measurements were performed by scanning 2θ, and the incident X-ray energy was 35 keV. The intensities change little with the channel number, but the FWHM slightly increases at the edge of the module (near channel 1280). This increasing trend is mainly due to the parallax errors because the high-energy X-ray diffraction beam traverses 1 mm of the Si sensor. The errors depend on the X-ray energy, and the observed maximum error is of the order of 6×10^{-4} (°) at 35 keV. In addition to this effect, anomalous counting is observed at the edges of each module. Similar phenomena were observed in a past study.[21] In order to avoid such anomalous counting effects for the diffraction data, we did not use the data of 20 channels from the edges of each module. Therefore, the active overlap regions

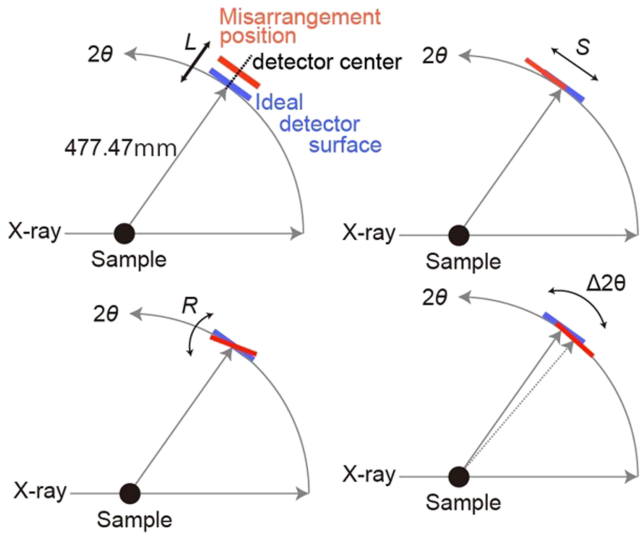

FIG. 3. Schematics of the parameters related to 2θ errors in the MYTHEN modules due to both the flat detector surfaces and mechanical misarrangement of the detectors.

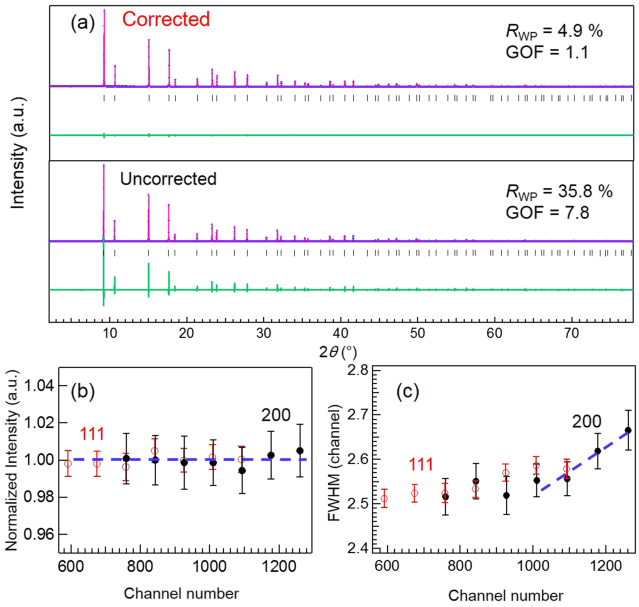

FIG. 4. (a) Whole pattern fitting results of the CeO_2 sample before and after 2θ correction. Observed (b) integrated intensities and (c) FWHM for each Bragg reflection of CeO_2 as a function of channel. The reflections were fitted by Gaussian profile functions.

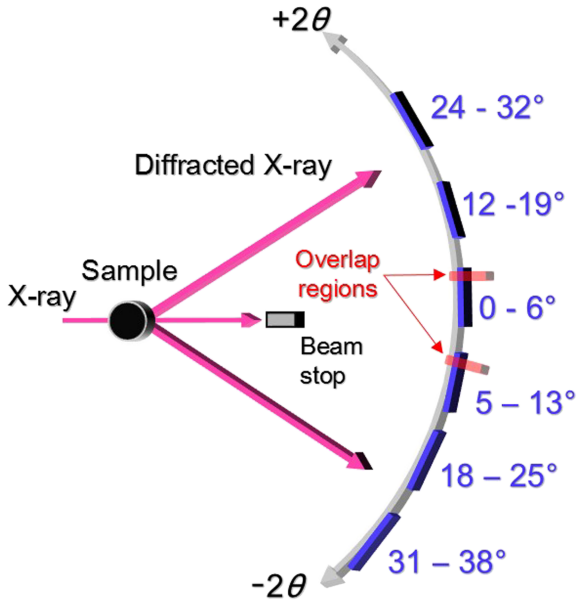

FIG. 5. Detector arrangement in the single-step mode.

are approximately 1.2° in 2θ. To merge the diffraction data measured at the first and second positions for the double-step mode, the scaling factors among the modules were calculated by the integrated intensities in the overlap regions. The deviations of the scaling factor among all modules were less than approximately 1% because of the difference in efficiency of each module. In order to avoid the effect of the reduction of parallax errors, data reduction from all modules was switched at approximately the middle position between the first and second positions for the double-step mode, as shown in the inset of Fig. 2(a). This 2θ region is omitted in the merged powder diffraction pattern, which is not used for the final diffraction pattern. The 2θ region between the switched position and an edge of the module is approximately 0.7°. These corrections for the 2θ angles and intensities were carried out at the first run. Therefore, users are able to obtain the corrected datasets. The 2θ angles of raw data from 1-D flat detector are not equivalent interval. A piece of software for powder diffraction cannot treat this type of raw data. Therefore, the developed data reduction software was able to correctly change the equivalent step to 0.006° with intensity by the linear interpolation function. In this study, the equivalent step data are used for all diffraction patterns.

Next, we introduced another method, which is referred to as the "single-step mode" in this report, in which data are recorded simultaneously at 2θ values ranging from 2° to 38° in the single-shot measurement. The 2θ range covered by each module is indicated in Fig. 5. The gaps between modules in the positive 2θ region can be detected by the modules in the negative 2θ region. For example, the dead area from 6° to 12° in the positive 2θ region can be collected by the region from 5° to 13° in the negative 2θ region. In both the positive and negative 2θ sides, there are overlapping regions in 2θ as well as the data in the double-step mode. Hence, it is possible to perform data reduction for the whole pattern similar to the double-step mode. In this detector arrangement, the adjustment of the beam stop is very important because the direct X-ray beam can directly hit the MYTHEN module if the adjustment is missed. Typically, the detectors in the double and single step modes can be counted from 2θ = 2°. Hence, the measurable minimum Q-range is from 0.2 to 0.65 $Å^{-1}$ for X-ray energies ranging from 12 to 37 keV. The measurement technique with the detector arrangement used here was developed by Katsuya and Sakata.[21] The single-step mode is very suitable for time-resolved and/or *in operando* powder diffraction measurements since it is not necessary to fill in the detector gap by moving the 2θ axis. The acquisition time is less than half in the double-step mode because it is not necessary to collect for the double step and to move the detector along the 2θ axis. Hence, this single-step measurement can be useful for the structural investigation of the dynamical changes of the sample environment (e.g., temperature, time, and pressure). In the double-step mode, an equivalent sample environment for the first and second scans is necessary for the measurement, but the advantage of the double-step mode is that the high Q datasets can be obtained. The double-step diffraction data are suitable for static structural investigation, and structural refinements are generally carried out by whole patterns recorded with large Q ranges. Additionally, one can easily switch between double- and single-step measurement modes just by moving the 2θ axis by approximately 40°.

The IP detector (Fuji BAS IP SR 2040) can also be used for powder diffraction experiments on the developed system. The powder diffraction data can be read out using a Fuji BAS 2500. The configuration of the IP detector is displayed in Fig. 1(b). In general, the advantageous features of the IP are as follows: low cost and large active area size, 2D detector, and higher efficiency for high-energy X-rays. As mentioned above, the MYTHEN has better angular resolution and high dynamical range than the IP in the developed system, but

the quantum efficiency of the MYTHEN for X-ray energies $E > 30$ keV is less than 25%, and its efficiency falls to 10% at 40 keV, even if the thickness is 1 mm. This low efficiency increases the data acquisition time. Moreover, the IP detector with a large active area can collect continuous diffraction data with a large Q range over 20 Å^{-1} at 35 keV in the single-shot measurement, whereas at least two exposures are required for the MYTHEN detectors. Using high-energy X-rays ($E \geq 35$ keV), the data collection time for the IP detector is roughly half or one-third shorter than that for the MYTHEN detectors. Thus, the IP detector can be easily applied in structural studies requiring high-energy X-rays, e.g., charge-density and pair distribution function analyses. Additionally, the 2D powder pattern can be useful for the evaluation of crystal grains in powder specimens.

III. HIGH THROUGHPUT MEASUREMENT SYSTEM

We developed a compact and easy-to-handle auto-sampler, which does not affect the temperature control, and incorporated it into the multi-MYTHEN-detector diffractometry system. This measurement system can perform the SR-XRPD measurement fully automatically. The auto-sampler is depicted in Figs. 6(a) and 6(b). Sample exchange, including the capillary alignment system, can be performed rapidly, within approximately 1 min per sample. A total of 30 samples can be mounted on the sample pallet, which is easily detachable from the auto-sampler. The switch of the capillary sample is performed via motion along the four axes of the sampler, X_r, Y_r, Z_r, and *Rot*. An arbitrary sample is carried by the Y_r- and Z_r-axes to grasp it by a robotic hand and is transported to the ω-sample stage along the X_r- and *Rot*-axes. The robotic hand is controlled (i.e., opened or closed) by compressed air with a pressure of 0.5 MPa. Next, we developed an automatic capillary sample alignment system in order to correctly irradiate the sample with the X-ray beam. The alignment system is designed to move the sample stage in five ways: via translation along the Y- and Z-axes, adjustment of the RZ and RY tilt angles, and rotation in the φ-direction. Note that the tilt axes can modify the slope of the capillary sample for the X-ray beam, where the sample is arranged perpendicular to the X-ray beam with a width of 3 mm. A microscope with a charge-coupled device (CCD) camera serves as an image recognition system and can recognize the edges of capillary images based on the contrast observed through the CCD. The sample can thereby be moved to the center of the diffractometer. After the capillary sample is precisely mounted on the sample stage, the sample spins continuously by the φ-axis until all the necessary measurements have been acquired in order to improve the intensity homogeneity along the Debye–Scherrer rings for accurate peak intensity measurements. The oscillation of the ω-axis can be utilized during the measurement instead of that of the φ-axis.

The sample temperature is controlled by low- or high-temperature N_2 gas streams produced by a device that can achieve rapid heating/cooling at a rate of 80 K/min. The available temperature ranges for the low- and high-temperature devices are 90–573 K and 300–1173 K, respectively. The automatic measurements can be easily controlled by loading the measurement conditions (e.g., sample number, temperature, and acquisition time) from an Excel file into the developed software. After that, the N_2 gas-stream device stage automatically moves close to the sample position. The temperature dependences from 90 to 1173 K of the measurement can be performed automatically. The low- and high-temperature N_2 gas-stream devices automatically change

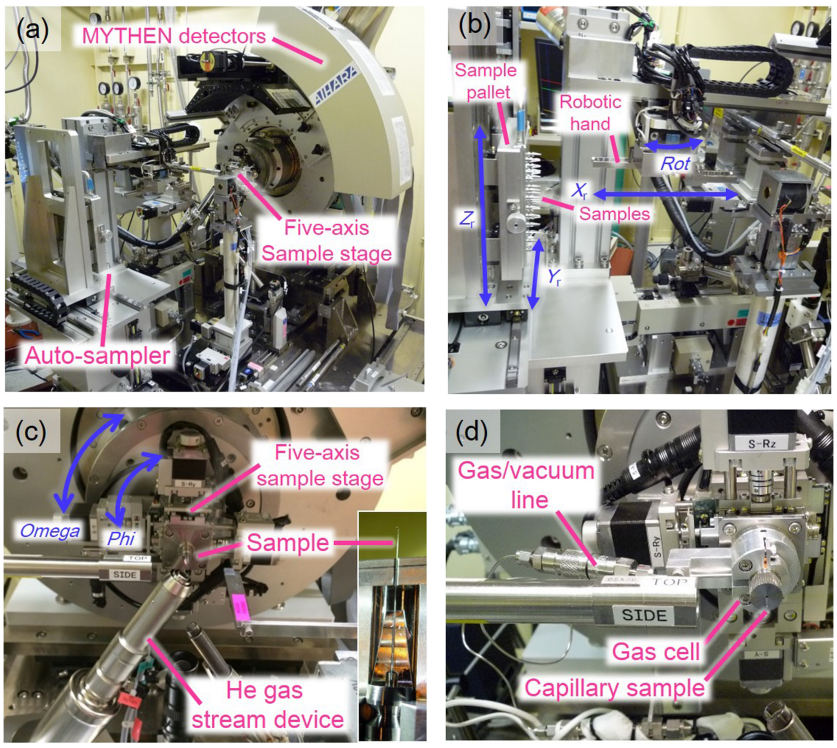

FIG. 6. (a) Photograph of the powder diffractometer consisting of six MYTHEN detectors and an auto-sampler. (b) Details of the auto-sampler. Photographs of the (c) five-axis sample stage, sample holder, He gas stream device, and (d) capillary gas cell (MicrotracBEL Corp.) mounted on the sample stage. The capillary with diameters of 0.4 mm and 0.5 mm can be used for this gas cell.

when the sample is ambient temperature. Hence, our new SR-XRPD system can be used to perform automatic measurements of Debye–Scherrer geometry using the capillary sample, including sample mounting/unmounting, capillary alignment, variable-temperature measurement over a wide-range of temperatures, and high-throughput data collection by MYTHEN detectors. Furthermore, switching between the MYTHEN system and IP detectors can be easily handled (within 1 min) just by moving the two-axis goniometer position and the 2θ axis without the need to perform a complicated diffractometer alignment. The two kinds of detectors and two measurement (Double- and Single-step) modes in the MYTHEN system can be quickly and selectively used for many kinds of requests from users. Thus, we successfully constructed a high-throughput and user-friendly powder diffraction system.

In addition, our system can be used to perform powder diffraction measurements under many kinds of sample environments. The cold He gas stream device pictured in Fig. 6(c) (Japan Thermal Engineering Co., Ltd.) offers a temperature range of 25–300 K. Cold He gas is supplied by the cryostat connected with He gas bottles, in which it is not necessary to use liquid He. A closed-type cryostat is often used in low-temperature diffraction experiments. In this case, the sample exchange procedure not only takes a long time because the cryostat needs to warm up to room temperature but it is also complicated for beginners. For the He gas stream device, sample exchange is easy to handle even at 25 K, without having to heat the samples up to room temperature. Therefore, this user-friendly device facilitates rapid measurement at low-temperatures, which should be very useful in physical and chemical science fields. In contrast, for high-temperature experiments, furnaces with capillary extension equipment (HTK1200N, Anton Paar Co., Ltd.) are available at the beamline. The maximum attainable temperature is 1473 K, and the heating/cooling rate is high (50 K/min). This temperature device enables accurate and/or *in situ* structural studies of solids and liquids to be performed even at 1473 K. For these temperature control devices, the temperatures at sample position were calibrated by the thermocouple device (K-type). The calibration table was prepared at the beamline.

In order to control gas atmosphere (i.e., O_2, H_2, N_2, CO_2, Ar, and He) and pressure for the sample in the glass capillary, we developed the gas handling system shown in Fig. 6(d), automatically controlled by the operation PC. This system consists of a digital mass flow controller, air valves, electronic vacuum gages, and a turbo-molecular pump. The gas pressure and flow rate for the sample in the capillary can be automatically controlled in the 0.1 Pa–130 kPa pressure range by the software connected to the MYTHEN measurement system, which was developed using the LABVIEW software package. These user-friendly instruments make it possible to measure *in situ* powder diffraction not only over an extended temperature range from 25 K to 1473 K but also in many kinds of gas atmospheres or vacuum.

IV. PERFORMANCE

All the powder diffraction data for the SRM CeO_2 obtained using the multi-MYTHEN-detector system in double-step mode were least-squares fitted based on the Rietveld method, as shown in Fig. 7(a). The wavelength of the incident X-rays was 0.499 575(1) Å, and the threshold energies of the MYTHEN detectors were set to half of the incident X-ray energy in all of the measurements. The powder diffraction data obtained with acquisition times of 60 s were analyzed using the JANA2006 software program.[22] All the diffraction peaks were fitted by applying conventional pseudo-Voigt profile functions. The reliability indices of the Rietveld refinements were a weighed profile R-factor (R_{wp}) of 0.062, Bragg intensity R-factor (R_I) of 0.015, and goodness-of-fit (GOF) of 1.03. The isotropic atomic displacement parameters U_{iso} were 0.002 97(2) and 0.0054(1) for the Ce and O atoms, respectively. Figure 7(b) presents the observed powder diffraction profile of the SRM Si 640c. The 311 peak profile is symmetric and narrow, with $\Delta 2\theta = 0.0178°$. The 2θ step angle 0.006° makes the peak shape slightly triangular at low 2θ values. In this study, the step angle is slightly larger than one-third of the FWHM. This issue originates from the fixed strip size of the MYTHEN and good pixel spread function of each strip. Therefore, the fitting accuracy is slightly poor at low diffraction angles. A similar phenomenon is observed at the other beamlines on the diffraction data of NIST fluoride $Na_2Ca_3Al_2F_{14}$.[16] However, this effect is negligible for the majority of samples because the intrinsic peak widths are normally larger than that for the NIST samples. The FWHM as a function of the 2θ values of the recorded diffraction peaks is depicted in Fig. 7(c). The FWHM increases almost linearly without any

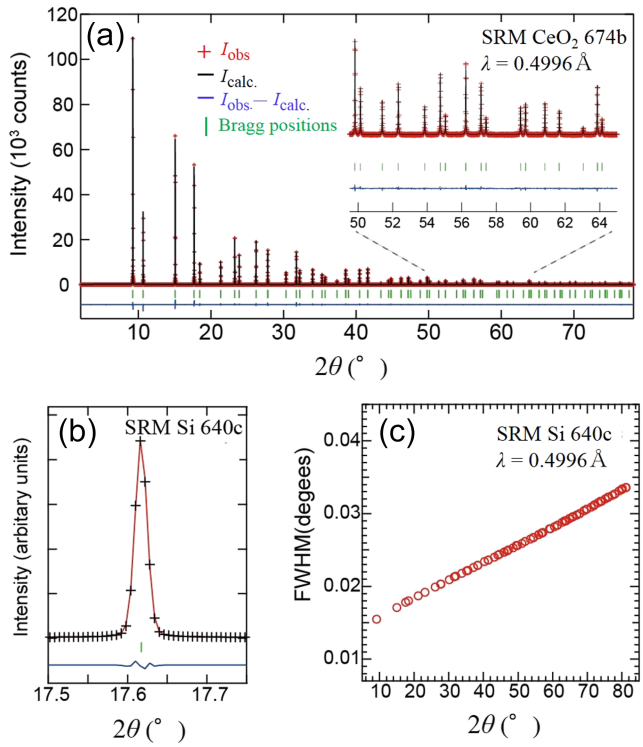

FIG. 7. (a) Rietveld refinements of CeO_2 powder. (b) Si 311 reflection profile fitting results. (c) FWHM as a function of 2θ of Si powder. The CeO_2 and Si powder specimens were loaded in Lindeman glass capillaries with diameters of 0.1 mm and 0.2 mm, respectively. In order to reduce the sample absorption effect for the intensities from the cylindrical crystals, which is less than 1% at $2\theta = 70°$, we used the small capillary sizes.

discontinuity and provides a low value of $\Delta 2\theta$ (0.03°) when 2θ is large. In the Debye–Scherrer geometry, the dependence of the FWHM on the diffraction angle is affected by the X-ray optics, and instrumental and microstructural broadenings.[7,16] In our beamline, the energy resolution $\Delta E/E$ of incident X-rays was approximately 2×10^{-4}. Therefore, the peak width at 0.02° – −0.03° and high 2θ angles is generally larger than that at low 2θ angles. The broadening for diffraction angles is mainly due to the X-ray optics.

Using the automatic measurement system, *in situ* powder diffraction measurements for the corundum-type V_2O_3 and Ti_2O_3 compounds were performed in the single-step mode. The powder pattern acquisition times were 5 s and 15 s for V_2O_3 and Ti_2O_3 per frame, and an X-ray energy of 22 keV was used. The measurable Q ranges ($0.4 \le Q \le 7.2$ Å^{-1}) for each datum are approximately equivalent to the case of the diffraction pattern in the range of $5° \le 2\theta \le 120°$ measured by the Cu$K\alpha$ source. The sample temperature was controlled from 100 K to 200 K for V_2O_3 and from 300 K to 750 K for Ti_2O_3 by the low- and high-temperature N_2 gas stream devices, and the temperature increased approximately 5 K/min during data collection. The obtained diffraction patterns as a function of temperature are displayed in Fig. 8. The 2D plot of the powder patterns for V_2O_3 reveals a structural phase transition from hexagonal to monoclinic at approximately 160 K. In contrast, for Ti_2O_3, the peak positions of the (110) and (104) Bragg reflections show a kink at approximately 500 K, indicating a structural phase transition. These structural transitions are well known as the metal–insulator phase transitions.[23,24] All of the diffraction data were rapidly acquired (within 5 s and 15 s for V_2O_3 and Ti_2O_3) single-shot measurements. The developed diffractometer system can perform these *in situ* measurements on the temperature dependence of the powder diffraction pattern in a short time (20 min and 90 min for V_2O_3 and Ti_2O_3).

To test the structural refinement of a metal-organic framework complex, we selected a nanoporous Cu coordination polymer $\{[Cu_2(pzdc)_2(pyz)]_n$ (pzdc = pyrazine-2,3-dicarboxylate; pyz = pyrazine)} (CPL-1) with a pillared layer structure containing 1D nanochannels with dimensions of 4.0 Å × 6.0 Å along the a-axis between 2D sheets.[10] This compound can adsorb various gases, and the maximum entropy/Rietveld method revealed the formation of a 1D array of molecular oxygen in the nanochannels. We performed *in situ* powder diffraction experiments of O_2 gas adsorption at 95 K. During data collection, the pressure in the cell was controlled under 90 kPa by the developed gas handling system. The powder pattern of CPL-1 was collected in double-step mode with an acquisition time of 600 s using a 15.5 keV X-ray beam. The final refinement results are presented in Fig. 9. The overall values of R_{wp} and R_F were 0.040 and 0.034, respectively. The Rietveld refinement was carried out using the GSAS software,[21] and the details of this process for CPL-1 are described in a previous work.[25] In Fig. 9, an array of molecular oxygen is observed in the nanochannels of CPL-1, a structure that had been previously reported.[26] However, here we could find the charge density induced by the adsorbed O_2 gas molecules on the difference Fourier map by using the general Rietveld refinement procedure. These

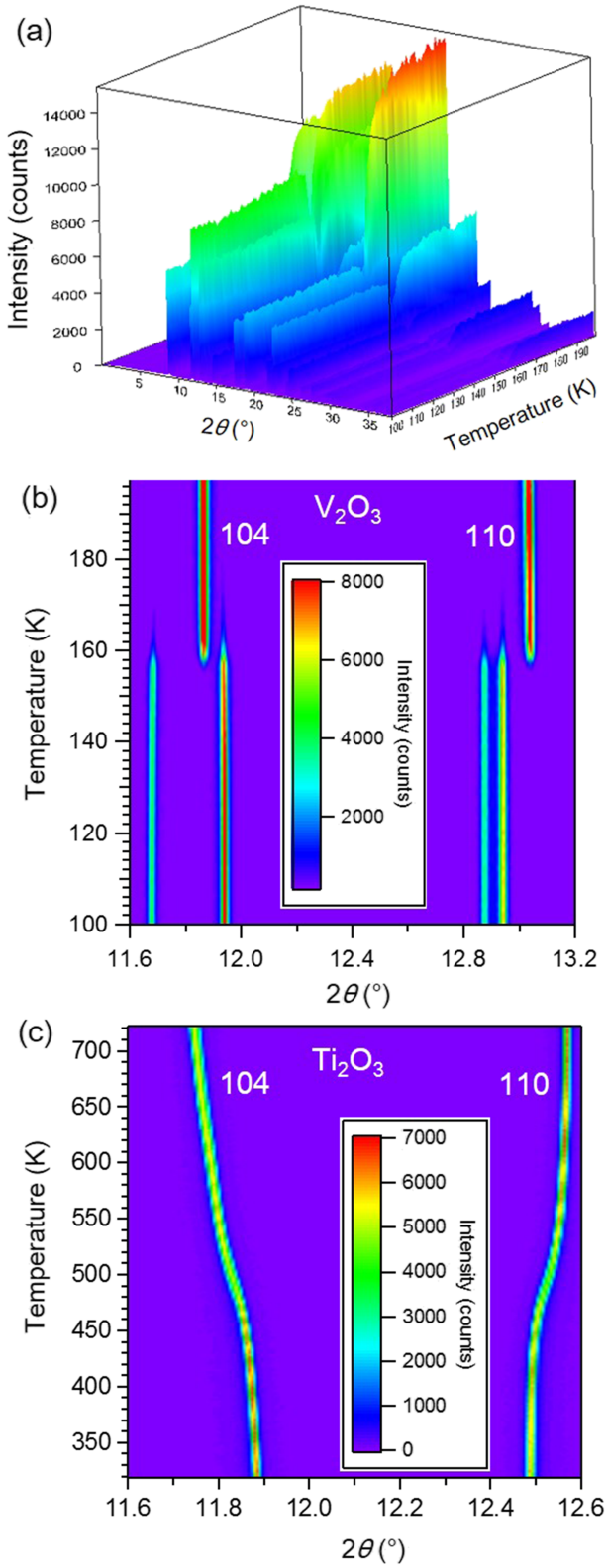

FIG. 8. (a) Temperature dependence of the patterns of V_2O_3 powders recorded in single-step mode. Two-dimensional plot of powder patterns for (b) V_2O_3 and (c) Ti_2O_3.

results demonstrated that the new multi-MYTHEN-detector system at beamline BL02B2 could acquire high-quality powder diffraction data for crystal structural analysis using the Rietveld method. The acquisition times of 30–180 s are

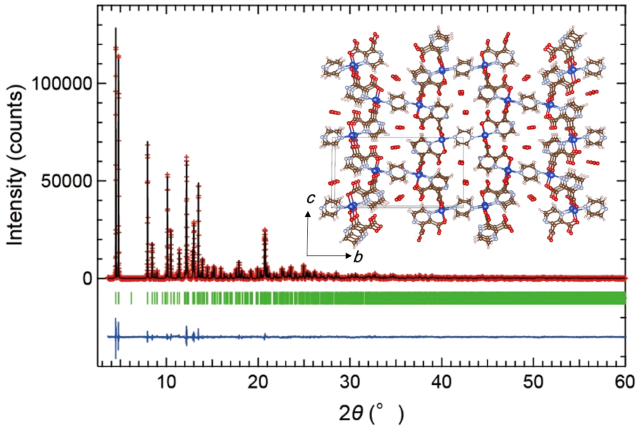

FIG. 9. Rietveld refinements of CPL-1 at 95 K in O_2 at 90 kPa. The inset shows the obtained crystal structure of CPL-1. The CPL-1 was loaded in the borosilicate glass capillary with a diameter of 0.5 mm.

sufficient for the structural refinement of inorganic materials. For organic materials, the acquisition times of 180–600 s are necessary. In addition, a few seconds of acquisition time can be used to observe the time dependences of the diffraction profiles. In fact, the details of the best acquisition time are determined by the incident X-ray energy, sample amount, and sample crystalline quality. Finally, let us mention that many structural investigations on various compounds, e.g., manganese perovskite oxides,[27] piezoelectric ceramics including heavy atoms,[28] carbon-rich active materials with macrocyclic nanochannels,[29] and molecular-based porous materials,[30] have been already performed using the developed diffractometer system.

V. CONCLUSION

The design and performance of a powder diffractometer consisting of six MYTHEN detectors, a compact auto-sampler, and wide-range temperature control systems at beamline BL02B2 of SPring-8 were described in this report. The MYTHEN detector system proved capable of obtaining high-resolution powder patterns in a fraction of a second. We also developed two data collection techniques. One is a single-step mode in which powder diffraction patterns can be collected in single shots, while the other is a double-step mode that can be used to acquire patterns with wider 2θ ranges. The new diffractometer system can automatically investigate the structural properties—such as the phase diagram—of up to 30 samples in a temperature range between 90 K and 1173 K. The new diffractometer system not only can accelerate scientific and industrial research but also allow performing SR-XRPD in a simple way by preparing samples in capillaries and an Excel file with the experimental conditions. The new attachments related to the sample environment can offer an extended temperature range between 25 K and 1473 K and various gas atmospheres and pressures. To calibrate the diffractometer, we used SRMs, namely, Si640c and CeO_2. The performance of the new powder diffractometer system was tested using V_2O_3, Ti_2O_3, and CPL-1. We found that the quality of the powder diffraction pattern is suitable for Rietveld refinement and *in situ* measurements. Our developed diffractometer system has these characteristics and is especially useful for performing automatic variable-temperature measurements with different, automatically controlled, gas atmospheres and pressures. In these experimental layouts, the IP detector can be also available. The switching between the MYTHEN system and IP detectors can be easily performed (within 1 min) without changing the experimental conditions before the switching. We believe that our powder diffractometer system will not only contribute to diverse scientific investigations, such as phase identification, structural determination, and charge-density studies, but also allow for *in situ* and/or time-resolved measurements for chemical reaction processes, gas storage, catalytic reactions, and battery charge/discharge.

ACKNOWLEDGMENTS

The synchrotron radiation experiments were performed at BL02B2 of SPring-8 with the approval of the Japan Synchrotron Radiation Research Institute (JASRI) (Proposal Nos. 2013B1925, 2013B1926, 2015A1434, 2015A2058, 2015B1988, 2016A1845, and 2016B1959). This work was supported by JSPS KAKENHI [Grant Nos. 16K17548, 2646005700, and 16H06514 (Coordination Asymmetry)] and the Hyogo Science and Technology Association. The authors thank Rigaku Aihara Precision Co., Ltd. for their help with the manufacture of the auto-sampler system. The authors also thank Professor R. Matsuda and Professor S. Kitagawa for their assistance with the sample preparation of CPL-1 and also thank Mr. T. Abe for his help.

[1] H. Toraya, H. Hibino, and K. Ohsumi, J. Synchrotron Radiat. **3**, 75 (1996).
[2] E. Nishibori, M. Takata, K. Kato, M. Sakata, Y. Kubota, S. Aoyagi, Y. Kuroiwa, M. Yamakata, and N. Ikeda, Nucl. Instrum. Methods Phys. Res., Sect. A **467-468**, 1045 (2001).
[3] A. N. Fitch, J. Res. Natl. Inst. Stand. Technol. **109**, 133 (2004).
[4] P. L. Lee, D. Shu, M. Ramanathan, C. Preissner, J. Wang, M. A. Beno, R. B. Von Dreele, L. Ribaud, C. Kurtz, S. M. Antao, X. Jiao, and B. H. Toby, J. Synchrotron Radiat. **15**, 427 (2008).
[5] M. Tanaka, Y. Katsuya, and A. Yamamoto, Rev. Sci. Instrum. **79**, 075106 (2008).
[6] S. P. Thompson, J. E. Parker, J. Potter, T. P. Hill, A. Birt, T. M. Cobb, F. Yuan, and C. C. Tang, Rev. Sci. Instrum. **80**, 075107 (2009).
[7] T. Straasø, J. Becker, B. B. Iversen, and J. Als-Nielsen, J. Synchrotron Radiat. **20**, 98 (2013).
[8] C.-R. Wang, T. Kai, T. Tomiyama, T. Yoshida, Y. Kobayashi, E. Nishibori, M. Takata, M. Sakata, and H. Shinohara, Nature **408**, 426 (2000).
[9] Y. Kuroiwa, S. Aoyagi, A. Sawada, J. Harada, E. Nishibori, M. Takata, and M. Sakata, Phys. Rev. Lett. **87**, 217601 (2001).
[10] R. Kitaura, S. Kitagawa, Y. Kubota, T. C. Kobayashi, K. Kindo, Y. Mita, A. Matsuo, M. Kobayashi, H.-C. Chang, T. Ozawa, M. Suzuki, M. Sakata, and M. Takata, Science **298**, 2358 (2002).
[11] E. Nishibori, E. Sunaoshi, A. Yoshida, S. Aoyagi, K. Kato, M. Takata, and M. Sakata, Acta Crystallogr., Sect. A: Found. Crystallogr. **63**, 43 (2007).
[12] B. Schmitt, C. Brönnimann, E. F. Eikenberry, F. Gozzo, C. Hörmann, R. Horisberger, and B. Patterson, Nucl. Instrum. Methods Phys. Res., Sect. A **501**, 267 (2003).
[13] F. Gozzo, B. Schmitt, Th. Bortolamedi, C. Giannini, A. Guagliardi, M. Lange, D. Meister, D. Maden, P. Willmott, and B. D. Patterson, J. Alloys Compd. **362**, 206 (2004).
[14] B. Schmitt, Ch. Brönnimann, E. F. Eikenberry, G. Hülsen, H. Toyokawa, R. Horisberger, F. Gozzo, B. Patterson, C. Schulze-Briese, and T. Tomizaki, Nucl. Instrum. Methods Phys. Res., Sect. A **518**, 436 (2004).

[15]A. Bergamaschi, A. Cervellino, R. Dinapoli, F. Gozzo, B. Henrich, I. Johnson, P. Kraft, A. Mozzanica, B. Schmitt, and X. Shi, Nucl. Instrum. Methods Phys. Res., Sect. A **604**, 136 (2009).
[16]A. Bergamaschi, A. Cervellino, R. Dinapoli, F. Gozzo, B. Henrich, I. Johnson, P. Kraft, A. Mozzanica, B. Schmitt, and X. Shi, J. Synchrotron Radiat. **17**, 653 (2010).
[17]R. G. Haverkamp and K. S. Wallwork, J. Synchrotron Radiat. **16**, 849 (2009).
[18]S. P. Thompson, J. E. Parker, J. Marchal, J. Potter, A. Birt, F. Yuan, R. D. Fearn, A. R. Lennie, S. R. Street, and C. C. Tang, J. Synchrotron Radiat. **18**, 637 (2011).
[19]M. Yamakata, S. Goto, T. Uruga, K. Takeshita, and T. Ishikawa, Nucl. Instrum. Methods Phys. Res., Sect. A **467-468**, 667 (2001).
[20]M. Tanaka, Y. Katsuya, Y. Matsushita, and O. Sakata, J. Ceram. Soc. Jpn. **121**, 287 (2013).
[21]Y. Katsuya, C. Song, M. Tanaka, K. Ito, Y. Kubo, and O. Sakata, Rev. Sci. Instrum. **87**, 016106 (2016).
[22]V. Petříček, M. Dušek, and L. Palatinus, Z. Kristallogr. - Cryst. Mater. **229**, 345 (2014).
[23]N. F. Mott and L. Friedman, Philos. Mag. **30**, 389 (1974).
[24]M. Imada, A. Fujimori, and Y. Tokura, Rev. Mod. Phys. **70**, 1039 (1998).
[25]A. C. Larson and R. B. Von Dreele, Los Alamos National Laboratory Report LAUR-86-748, 2000.
[26]K. Sugimoto, S. Kawaguchi, and M. Takemoto, "Structural characterization of caffeine–oxalic acid co-crystals from the powder diffraction pattern at the SPring-8 BL02B2 beamline," Powder Diffr. (published online 2017).
[27]I. Yamada, H. Fujii, A. Takamatsu, H. Ikeno, K. Wada, H. Tsukasaki, S. Kawaguchi, S. Mori, and S. Yagi, Adv. Mater. **29**, 1603004 (2017).
[28]I. Fujii, R. Iizuka, Y. Nakahira, Y. Sunada, S. Ueno, K. Nakashima, E. Magome, C. Moriyoshi, Y. Kuroiwa, and S. Wada, Appl. Phys. Lett. **108**, 172903 (2016).
[29]S. Sato, A. Unemoto, T. Ikeda, S. Orimo, and H. Isobe, Small **12**, 3381 (2016).
[30]I. Hisaki, S. Nakagawa, N. Ikenaka, Y. Imamura, M. Katouda, M. Tashiro, H. Tsuchida, T. Ogoshi, H. Sato, N. Tohnai, and M. Miyata, J. Am. Chem. Soc. **138**, 6617 (2016).